

AD 725469

NRL Report 7256

# Anodic Crystallization on Pure and Antimonial Lead in Sulfuric Acid

JEANNE BURBANK

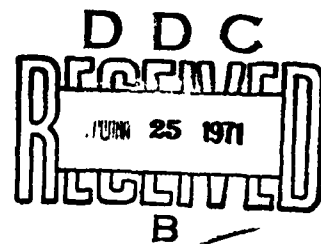
*Electrochemistry Branch  
Chemistry Division*

May 24, 1971



Reproduced by  
NATIONAL TECHNICAL  
INFORMATION SERVICE  
Springfield, Va. 22151

NAVAL RESEARCH LABORATORY  
Washington, D.C.



Approved for public release; distribution unlimited.

Security Classification		
DOCUMENT CONTROL DATA - R & D		
Security classification of title, body of abstract and indexing annotation must be entered when the overall report is classified		
1. ORIGINATING ACTIVITY (Corporate author)		2a. REPORT SECURITY CLASSIFICATION
Naval Research Laboratory Washington, D.C. 20390		Unclassified
3. REPORT TITLE		2b. GROUP
ANODIC CRYSTALLIZATION ON PURE AND ANTIMONIAL LEAD IN SULFURIC ACID		
4. DESCRIPTIVE NOTES (Type of report and inclusive dates)		
An interim report on a continuing NRL problem.		
5. AUTHOR(S) (First name, middle initial, last name)		
Jeanne Burbank		
6. REPORT DATE	7a. TOTAL NO OF PAGES	7b. NO OF REFS
May 24, 1971	32	73
8a. CONTRACT OR GRANT NO	9a. ORIGINATOR'S REPORT NUMBER(S)	
NRL Problem C05-14	NRL Report 7256	
b. PROJECT NO	9b. OTHER REPORT NO(S) (Any other numbers that may be assigned this report)	
Project RR 010-01-45-4755		
c.		
d.		
10. DISTRIBUTION STATEMENT		
Approved for public release; distribution unlimited.		
11. SUPPLEMENTARY NOTES		12. SPONSORING MILITARY ACTIVITY
		Department of the Navy (Office of Naval Research), Arlington, Virginia 22217
13. ABSTRACT		
<p>Electrochemical cycling, x-ray diffraction, and electron microscopy were used to study anodic crystallization on pure and antimonial Pb in <math>H_2SO_4</math>. On pure Pb a maximum electrochemical capacity developed that did not increase with further cycling. The anodic coating was comprised of small needlelike crystals that grew with cycling. The amount and crystallinity of <math>\beta PbO_2</math> gradually increased in a soft porous outer layer. Attached to the metal was a layer of <math>\alpha PbO_2</math>. On the Sb-Pb alloy the capacity continually increased with cycling. A compact eutectoidal coating of small crystals of <math>\alpha</math> and <math>\beta PbO_2</math> was formed. It was concluded that on pure Pb <math>\beta PbO_2</math> does not bond to <math>\alpha PbO_2</math> and that Sb in the Sb-Pb alloy acts as a nucleating catalyst for <math>\beta PbO_2</math> in the corrosion product attached to the metal surface. Antimony also promotes intercrystal bonding between the two polymorphs of <math>PbO_2</math>.</p> <p>The morphologies of the <math>PbSO_4</math> crystals were also studied. The crystals formed on soaking in the electrolyte, and during discharge of <math>PbO_2</math> coatings, developed by electrochemical cycling, were examined. Well-developed prisms, dendrites, and hopper crystals were observed. The discharge of the antimonial coatings appeared to be limited by the growth rate of the <math>PbSO_4</math> crystals.</p> <p>The fundamental aspects of electrocrystallization are discussed, and a crystal chemical mechanism is proposed for the action of Sb in the <math>PbO_2</math> electrode. A broad program for future investigation is outlined.</p>		

KEY WORDS	LINK A		LINK B		LINK C	
	ROLE	WT	ROLE	WT	ROLE	WT
Lead-acid cell Lead antimony alloys Pure lead Lead dioxide Lead sulfate Anodic corrosion Products Crystal morphology Electron microscopy Antimony						

## CONTENTS

Abstract	ii
Problem Status	ii
Authorization	ii
INTRODUCTION	1
RECENT EXPERIMENTAL WORK	2
Anodization and Cycling	2
Replication of the Anodic Products for Electron Microscopy	2
RESULTS AND DISCUSSION	5
Discharge Capacities	5
X-Ray Analyses	6
Morphology	8
A Proposed Mechanism for the Beneficial Action of Antimony on the Stabilization of Polycrystalline Lead Dioxide	16
Some Crystal Chemistry Considerations	20
An Outline for Future Investigations	24
ACKNOWLEDGMENT	24
REFERENCES	25

## ABSTRACT

Electrochemical cycling, x-ray diffraction, and electron microscopy were used to study anodic crystallization on pure and antimonial Pb in  $\text{H}_2\text{SO}_4$ . On pure Pb a maximum electrochemical capacity developed that did not increase with further cycling. The anodic coating was comprised of small needlelike crystals that grew with cycling. The amount and crystallinity of  $\beta\text{PbO}_2$  gradually increased in a soft porous outer layer. Attached to the metal was a layer of  $\alpha\text{PbO}_2$ . On the Sb-Pb alloy the capacity continually increased with cycling. A compact eutectoidal coating of small crystals of  $\alpha$  and  $\beta\text{PbO}_2$  was formed. It was concluded that on pure Pb  $\beta\text{PbO}_2$  does not bond to  $\alpha\text{PbO}_2$  and that Sb in the Sb-Pb alloy acts as a nucleating catalyst for  $\beta\text{PbO}_2$  in the corrosion product attached to the metal surface. Antimony also promotes inter-crystal bonding between the two polymorphs of  $\text{PbO}_2$ .

The morphologies of the  $\text{PbSO}_4$  crystals were also studied. The crystals formed on soaking in the electrolyte, and during discharge of  $\text{PbO}_2$  coatings, developed by electrochemical cycling, were examined. Well-developed prisms, dendrites, and hopper crystals were observed. The discharge of the antimonial coatings appeared to be limited by the growth rate of the  $\text{PbSO}_4$  crystals.

The fundamental aspects of electrocrystallization are discussed, and a crystal chemical mechanism is proposed for the action of Sb in the  $\text{PbO}_2$  electrode. A broad program for future investigation is outlined.

## PROBLEM STATUS

This report covers one phase of the investigation; work on other phases is continuing.

## AUTHORIZATION

NRL Problem C05-14  
Project RR 010-01-45-4755

Manuscript submitted January 27, 1971.

## ANODIC CRYSTALLIZATION ON PURE AND ANTIMONIAL LEAD IN SULFURIC ACID

### INTRODUCTION

The  $\text{PbO}_2$  electrode, with a technology stretching back slightly more than 100 years, has been studied in considerable detail. Fundamental investigations of the system cross over many scientific disciplines, and the need for further research rests with the expanding demand for portable energy sources, for example, for pollution-free propulsion. The purpose of this report is to present some recent results of the experimental investigation of the  $\text{PbO}_2$  electrode, to propose a mechanism for the beneficial action of Sb in the electrode, to outline the fundamental aspects of the study, and to suggest a research program directed to finding a substitute for Sb. A substitute is desired because Sb is in short supply in the Western world, and in addition to its beneficial action, it is also detrimental, causing the self-discharge of both the  $\text{PbO}_2$  and Pb electrodes, as well as poisoning of the Pb electrode.

The  $\text{PbO}_2$  plates for the lead-acid cell are made by mixing a plasterlike paste of  $\text{PbO}$ ,  $\text{H}_2\text{O}$ , and  $\text{H}_2\text{SO}_4$ , and applying this paste to a rigid metallic grid of Pb alloy. Following the "setting" of the paste it is converted to  $\text{PbO}_2$  by electrochemical oxidation in  $\text{H}_2\text{SO}_4$ , and the plate is ready for use. Despite the apparent straightforward process indicated, many facets of the operation remain to be clarified in detail.

Because the  $\text{PbO}_2$  plate is usually the limiting plate as far as cell performance and life are concerned, it offers a most promising area for improvement. The anticipated improvements are (a) mechanically stronger active material plaques, (b) improved service life, (c) higher energy density, (d) thinner positive plates and/or, (e) thin-plate non-antimonial cells for cycle and float service.

Antimony is normally present in the cell as an alloying agent to stiffen the grids used to support the active materials. It is further recognized as contributing significantly to the successful cycle operation of the positive plate (1-3), where it acts as a nucleating catalyst for the  $\text{PbO}_2$ , promotes intercrystal bonding, and modifies the crystal size and habit. To continue the investigation of the mechanism of the action of Sb in the positive plate, the crystal habits of  $\text{PbO}_2$  and  $\text{PbSO}_4$  crystallizing on anodes of Pb-Sb alloy have recently been examined (4,5).

The anodic oxidation products forming on Pb and its alloys at potentials near the reversible  $\text{PbO}_2$ ,  $\text{PbSO}_4$  electrode in  $\text{H}_2\text{SO}_4$  have been identified by x-ray diffraction. At potentials above this electrode, an outer layer of the corrosion product has been identified as primarily  $\beta\text{PbO}_2$ , and an inner layer, closer to the metal, is primarily  $\alpha\text{PbO}_2$ , which is frequently intermixed with some  $\beta\text{PbO}_2$ . Tetragonal  $\text{PbO}$  and  $\text{PbSO}_4$  have been detected at lower potentials. The relative amounts of these materials in the corrosion layers depends on the polarization potential, length of anodic treatment, temperature, current density, concentration of the  $\text{H}_2\text{SO}_4$  electrolyte, and metal composition (6-8).

The anodic films formed on pure Pb have also been examined by electron microscopy. The individual crystals of  $\text{PbO}_2$  are usually very small, lying within the submicron range

that gives rise to some degree of x-ray line broadening, while the  $\text{PbSO}_4$  crystals observed on pure Pb anodes are generally much larger than the  $\text{PbO}_2$  crystallites (7,9-12).

The reaction at the positive plate of the lead-acid cell is particularly complicated because it involves dissolution and crystallization of two solid phases,  $\text{PbO}_2$  and  $\text{PbSO}_4$ , as well as the charge exchange reactions. The plate reaction takes place by way of solution in the  $\text{H}_2\text{SO}_4$  electrolyte (13,14); however, the solubilities of  $\text{PbSO}_4$  and  $\text{PbO}_2$  are very low. Despite these complexities, the electrode performs very well at relatively high current densities.

In the discharge of a  $\beta\text{PbO}_2$  electrode in  $\text{H}_2\text{SO}_4$  at constant current, the potential passes through a minimum (15), which is reflected in the cell voltage and is known as the coup de fouet or spannungssack. During this period the supersaturation of  $\text{Pb}^{2+}$  in the electrolyte is built up, and the critical nuclei of  $\text{PbSO}_4$  are formed (16,17). Growth of the  $\text{PbSO}_4$  crystals then follows at a lower polarization. This behavior is fairly typical of nucleation and growth kinetics in many electrocrystallization reactions (18,19).

Antimony is coprecipitated with  $\text{PbSO}_4$  to such a degree that it interferes with the gravimetric analytical procedure (20), and its separation from Pb is required for accurate results. Dawson et al. (21) recently suggested that, in  $\text{H}_2\text{SO}_4$  solutions, Sb is present as the anions  $\text{Sb}(\text{SO}_4)_2^-$ ,  $\text{SbOSO}_4^-$ , and  $\text{Sb}_3\text{O}_9^{3-}$ . Strong absorption on the crystal surface may be expected to result in an alteration in habit, growth rates, and lattice substitution in the growing crystals.

## RECENT EXPERIMENTAL WORK

### Anodization and Cycling

Aged castings of pure Pb and nominally 5% Pb-Sb alloy were used in this study. The spectrographic analyses of these metals are given in Table 1. The specimens measured approximately  $6 \times 3 \times 0.4$  cm and fit the sample holder of the x-ray diffractometer so that x-ray patterns could be registered without destruction of the sample. Immediately prior to use, the specimens were washed in saturated ammonium acetate solution and thoroughly rinsed in distilled  $\text{H}_2\text{O}$ . While wet with the final rinse, they were assembled in beaker cells containing two sheet Pb cathodes, a Hg,  $\text{Hg}_2\text{SO}_4$  reference electrode, and 4.4M  $\text{H}_2\text{SO}_4$ . The cells were allowed to stand on open circuit for 30 min before the anodic current of 1 mA/cm<sup>2</sup> was applied. The cell voltages and plate potentials were continuously recorded on strip charts and frequently checked manually with a potentiometer. Experiments were run in triplicate. The cycled samples were discharged at 1 mA/cm<sup>2</sup> to a potential of 0.75 to 0.8 V vs the reference electrode and recharged at the same current density. Anodization was continued between discharges. X-ray diffraction patterns were registered with  $\text{CuK}\alpha$  radiation, using the diffractometric method (22) with scanning speeds of 2° and 0.2°/min. The x-ray patterns were registered intermittently throughout the anodization periods, quite frequently in the early stages. Specimens for electron microscopy were removed at intervals, blotted dry, and replicated as soon as possible after concluding the anodic treatment. During discharge the interval known as the coup de fouet had a duration of approximately 5 min under these conditions and the minimum was reached at 3.25 min. Discharging electrodes were examined at 0.5, 2, 3.25, 4, and 5 min, 1 hour (half discharge capacity), and at the knee of the curve.

### Replication of the Anodic Products for Electron Microscopy

Various techniques are commonly used to replicate specimens for electron microscopy, and the method selected depends on the nature of the material under investigation. Evaporated carbon has found great favor as a final replica because of its chemical inertness,

Table 1  
Spectrographic Analysis of Metals  
Used in This Study

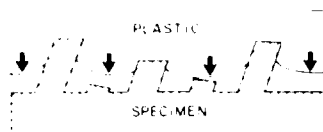
Element	Pure Lead	Antimony Alloy
Pb	VS	VS
Sb	VW	S
Bi	VW	W-M
Fe	VW	VW
Al	—	—
Ni	FTR	VW
Si	VW	VW
Sn	VW	TR
Mg	TR	TR
Mn	TR	TR
As	—	VW
Cd	VW	—
Cu	TR	TR
Ag	VW	VW

Key: VS = 10 to 100%  
S = 1 to 10%  
M = 0.1 to 1%  
W = 0.01 to 0.1%  
VW = 0.001 to 0.01%  
TR = 0.0001 to 0.001%  
FTR = 0.0001% or less.  
— = not detected.

its lack of self structure, and its ability to withstand bombardment by the electron beam (23). In previous electron microscopic examinations of  $PbO_2$ , both single-stage and two-stage replicas have been used (2,7,9-12). In this study, it was necessary to resort to the two-stage polystyrene-carbon technique because of the very rough surfaces of some of the anodic products. The primary impressions of the anodic coatings were made by placing thin polystyrene wafers on the dried electrode surfaces, covering them with glass slides, adding weights to the slides, and placing the assemblies in an oven preheated to 165°C. The weight is not critical; 0.5 to 1 kg/cm<sup>2</sup> effective pressure was used in this investigation. The length of time required to take such impressions depends on the heat capacity of the assembly, and for the samples used in this work one-half hour was necessary. This manner of replication resulted in no change in the corrosion products detectable by x-ray diffraction examination.

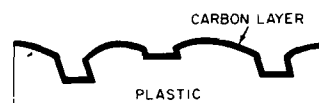
When the specimen has a high degree of surface relief, partial impressions are necessary because the plastic may totally encapsulate some features, and excessive undercutting renders final replication impossible. A partial impression, however, results in clear areas in the final replica where the softened plastic does not contact low-lying surface features, shown schematically in Fig. 1 and in the micrograph of Fig. 2. When the degree of surface relief is not excessive, the plastic will yield a complete replica of the surface as in the micrograph of Fig. 3.





(a) A partial impression of a surface with high relief. The arrows indicate areas that will be clear in the final replica. The low-lying features will not be shown. If the degree of surface relief is not excessive, the entire surface may be replicated.

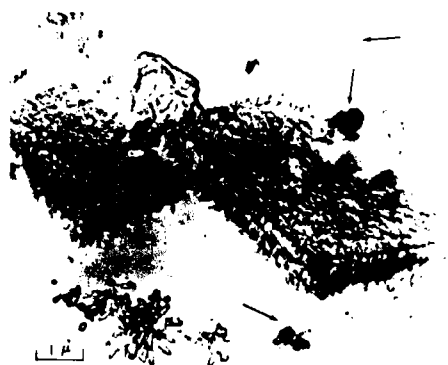
(b) Coating of evaporated carbon deposited on the plastic impression after the plastic is removed from the surface and cleaned of any adhering particles



(c) The final carbon replica rests on the grid wires of the specimen screen after removal of the plastic impression by dissolution

Fig. 1 - Diagram of the two-stage plastic carbon replication technique for electron microscopy. A primary impression of the specimen surface is obtained in softened plastic. If the surface has a high degree of relief, partial embedding is employed. After the plastic sets, it is pulled away from the surface and any embedded particles are removed by chemical or mechanical treatment. The impression is then rotary coated with evaporated carbon which forms the final replica and has the same topography as the original surface. The plastic is removed from the carbon film which is mounted on specimen screens for examination in the electron microscope.

Fig. 2 - Electron micrograph of the two-stage plastic carbon replica of the anodic corrosion product on pure Pb after seven cycles. Artifacts, indicated by the arrows, are the blank areas resulting from partial embedding in the original plastic, contamination with basic lead carbonate and stained residues. Despite these flaws, the replica is useful. The shape of the original  $\text{PbSO}_4$  crystal is assumed by the mass of small  $\text{PbO}_2$  crystallites that have replaced it. The individual crystals stand separated like bristles of a brush and are probably attached at their bases.



NOT REPRODUCIBLE

Fig. 3 - Electron micrograph of a carbon replica of the anodic product on Pb-Sb alloy after 23 cycles. This coating is made up of a compact layer of small crystals of  $\alpha$  and  $\beta$ PbO<sub>2</sub> with outgrowths of larger crystals. These may have resulted from small crystals originally oriented so that preferred growth planes were accessible to the solution. A relatively low degree of surface relief permits replication of the entire surface of the deposit.



NOT REPRODUCIBLE

Following the heating period required to form the primary impressions, the oven was turned off and the door opened carefully. It was allowed to remain slightly ajar until the undisturbed specimens cooled to room temperature. The polystyrene wafers were then pulled-away from the surfaces. Some particles of the corrosion products remained embedded in the replicas and were removed before the final carbon replica was prepared. The particles of corrosion product from pure Pb were readily dissolved by floating the polystyrene disks, particle side down, on HNO<sub>3</sub> or CH<sub>3</sub>COOH containing a few drops of H<sub>2</sub>O<sub>2</sub>. When Sb was present, however, a white insoluble residue formed in these solutions, which could not be removed from the plastic replicas.

The plastic replicas were examined with an optical microscope to determine when the adhering particles were removed, followed by thorough rinsing in distilled H<sub>2</sub>O and drying.

The polystyrene disks were then placed in a vacuum evaporator and rotary coated with carbon in the usual manner. The disks were cut into pieces slightly smaller than the specimen screens for the electron microscope. Each piece was placed, carbon side down, on a specimen screen, and the polystyrene was removed from the carbon replica by vapor washing with ethylene dichloride (24). The replicas were then examined in the electron microscope. Clearing the replicas from the antimonial specimens remains an art. By using oxalic acid to reduce the PbO<sub>2</sub> and tartrates to complex the Sb, the replica may be cleared. Occasional dips in H<sub>2</sub>SO<sub>4</sub> were used to precipitate PbSO<sub>4</sub>, which could then be removed in saturated ammonium acetate solution. By alternately treating with these reagents, rinsing with distilled H<sub>2</sub>O between the various baths, the formation of the curdy antimony oxide could be minimized. When all the PbO<sub>2</sub> had been reduced, HCl containing tartaric acid was used as a final treatment. The very stable insoluble antimony oxide gives rise to the chemical replica of Pb-Sb alloys (25) and interferes with the analytical chemistry of Sb (20).

## RESULTS AND DISCUSSION

### Discharge Capacities

The discharge capacities of the anodic corrosion films on both pure and antimonial Pb were 11 ma-hr/cm<sup>2</sup> at the beginning of anodic treatment and gradually increased with

electrochemical cycling. Initially the capacity developed on the Sb alloy was slightly less than that of the pure Pb specimens; however, after five or six cycles, the capacities of the antimonial coatings exceeded those developed on pure Pb. The discharge capacity of the Sb alloy continued to increase to a value of 7 mA-hr/cm<sup>2</sup> on the 23rd cycle, the duration of the cycle tests. The coating on pure Pb reached a maximum capacity of about 2.6 mA-hr/cm<sup>2</sup> beyond which it ceased to increase significantly, as shown in Fig. 4. These capacities were all measured at room temperature and at a discharge rate of 1 mA/cm<sup>2</sup> of apparent area. The curves shown in Fig. 4 indicate the general trend of the capacity increase with cycling. Owing to such factors as the change in true surface area, the measured values must be considered as giving orders of magnitude only.

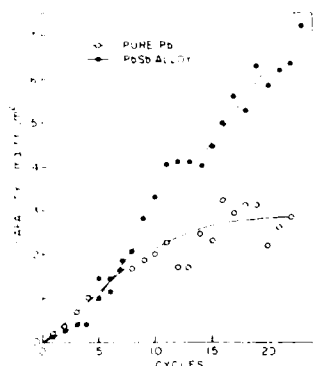


Fig. 4 - Capacity change with cycling of the anodic coatings on pure and antimonial Pb. The scatter in the data points is caused by uncontrolled variables, such as the change in surface area and mechanical loss of the coatings by shedding. The curves are representative of general trends for comparison purposes. The lower capacity on the Sb alloy at the start of cycling was observed in all runs and appears to be real. On pure Pb the capacity reaches a maximum and does not increase significantly with further cycling; on Sb alloy the capacity increases for the duration of the experiment.

#### X-Ray Analyses

X-ray diffraction examination of the pure Pb electrodes showed that the major product was tetragonal PbO at the earliest stage of anodic cycling. Detectable quantities of  $\alpha$  and  $\beta$ PbO<sub>2</sub> did not appear until after 20 hours of continuous anodic treatment. With cycling, the corrosion product became gradually richer in  $\alpha$  and  $\beta$ PbO<sub>2</sub>, and the outermost surface became mainly  $\beta$ PbO<sub>2</sub>. The intensity of the diffraction patterns of PbO<sub>2</sub> increased with cycling while the pattern of the underlying metal gradually became totally obscured as the coatings thickened. The outer layer was soft and powdery, shed slowly, and could be wiped from the surface. The underlying layer remaining on the electrode surface was almost entirely  $\alpha$ PbO<sub>2</sub>.

These observations suggest that when the discharge product PbSO<sub>4</sub> is recharged, the resulting  $\beta$ PbO<sub>2</sub> will not nucleate on nor grow attached to the underlying  $\alpha$ PbO<sub>2</sub> crystals. As a result, the  $\beta$ PbO<sub>2</sub> is loose and is readily detached from the surface of the pure Pb electrodes. This action appears to limit the discharge capacity that may be developed on the pure Pb electrodes.

On the Sb alloy, detectable quantities of  $\alpha$  and  $\beta$ PbO<sub>2</sub> developed in the anodic films after 2 hours anodization. The outer layer of the cycled corrosion product was mainly  $\beta$ PbO<sub>2</sub>. The coating increased in thickness with cycling and ultimately parted from the electrode surface in brittle flakes, leaving a microcrystalline coating of  $\alpha$  and  $\beta$ PbO<sub>2</sub> firmly attached to the metal surface. The outer surfaces of the flakes of corrosion product were mainly  $\beta$ PbO<sub>2</sub>, but the back of the layer was a mixture of  $\alpha$  and  $\beta$ PbO<sub>2</sub>. Therefore, Sb must serve to nucleate  $\beta$ PbO<sub>2</sub> in the corrosion product attached to the metal surface. When sufficient  $\beta$ PbO<sub>2</sub> is present in this primary film, the  $\beta$ PbO<sub>2</sub> resulting

from cycling can bond to the  $\beta\text{PbO}_2$  in the corrosion product film so that relatively thick layers are built up. An increase in the amount of  $\beta\text{PbO}_2$  in the anodic corrosion products of antimonial alloys has been reported by Levinson et al. (6), and Ritchie and Burbank (3) have suggested that Sb acts as a nucleating catalyst for  $\beta\text{PbO}_2$  in the positive active material of the lead-acid cell. Antimony also appears to promote intercrystal bonding between  $\alpha$  and  $\beta\text{PbO}_2$ .

During cycling of the electrodes, the so-called degree of crystallinity of the  $\text{PbO}_2$  increases more rapidly on pure Pb than on the antimonial alloy as evidenced by an increase in intensity of the diffraction pattern and the decrease in breadth of the diffraction lines. This comparison is clearly evident in the diffractometer traces shown in Fig. 5 in which the two patterns were recorded on the same chart under identical conditions. The low relative intensity and broad lines of the pattern from the anodic product on the Sb alloy is attributed to the small crystal size of the deposit, and to a greater degree of lattice distortion present in these crystals, which may be a result of substitutional solid solution of Sb in  $\text{PbO}_2$ . Similar differences in the degree of crystallinity of cycled active material on pure and antimonial lead have been reported by Kordes (1), Ritchie and Burbank (3), and others. The difference in the relative amounts of  $\alpha$  and  $\beta\text{PbO}_2$  in the two coatings is also apparent in the two traces, as well as in the deviation from standard relative intensities of the lines at  $25.4^\circ$  and  $32.03^\circ$  frequently observed in electrochemically prepared  $\text{PbO}_2$  (1,6).

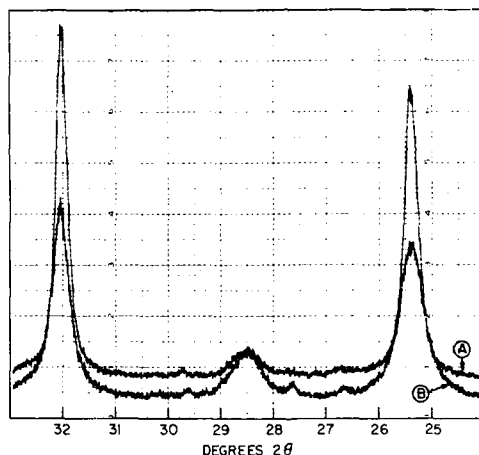


Fig. 5 - X-ray diffraction patterns over the range  $24^\circ$  to  $33^\circ$   $2\theta$  of the anodic coatings on pure and antimonial Pb after seven cycles. Pattern A was obtained from pure Pb, and pattern B was obtained from antimonial alloy. The patterns were superimposed by rewinding the chart after the first pattern had been recorded, displacing the rate meter zero by four small scale divisions, and leaving all other instrument settings the same. The scanning rate for these patterns was  $0.2^\circ$   $2\theta$ /min with  $\text{CuK}\alpha$  radiation and a full-scale deflection of 1000 counts per second. The major peaks arise from  $\alpha$  and  $\beta\text{PbO}_2$ , and both patterns show the line at  $32.03^\circ$  to be more intense than that at  $25.4^\circ$ . This is the reverse of the standard pattern for  $\beta\text{PbO}_2$  recorded by similar techniques. The pattern from the corrosion product on pure Pb has a higher intensity than that from the antimonial alloy. The width of the diffraction lines at half height is greater on the antimonial specimen, attributed to a smaller particle size for this deposit. The relative intensity of the peak at  $28.5^\circ$ , which arises from  $\alpha\text{PbO}_2$ , is lower on the pure Pb specimen than on the antimonial specimen, indicating that less of this material is present in the outer parts of the anodic coating.

### Morphology

**Lead Dioxide**—The uncycled anodic coatings formed on pure Pb at potentials above the  $\text{PbO}_2$ ,  $\text{PbSO}_4$  electrode showed outlines of  $\text{PbSO}_4$  crystals which had been replaced by very small needlelike crystals, Fig. 6. The small crystals were conglomerated within the outlines of the  $\text{PbSO}_4$  crystal bodies but did not exactly fill the original crystal volumes as would have been the case if the replacement had been a metasomatic process. In the early stages of anodic treatment, x-ray diffraction patterns indicated that the major component of the films was tetragonal  $\text{PbO}$ . The measurable discharge capacity exhibited by this coating suggests that the tetragonal  $\text{PbO}$  may be in the oxidized form described by Burbank (26,27).

Subsequent cycling increased the amount of  $\beta\text{PbO}_2$  on the electrode surface in a porous layer. This layer showed the gross outlines of  $\text{PbSO}_4$  crystals but appeared to be a hedgehog type of dendritic growth (Figs. 2 and 7). After 22 cycles, spheroidal conglomerates of  $\text{PbO}_2$  remained on the surface. These conglomerates were made up of larger anhedral crystals (Fig. 8).

On the antimonial alloy the initial uncycled coatings were also agglomerates of small crystals having the gross outlines of  $\text{PbSO}_4$  crystals similar to the coating observed on pure Pb in Fig. 6. Despite the similarity in morphology, in the case of the Sb alloy, x-ray diffraction showed that, after 2 hours of an anodic treatment, this coating was a mixture of  $\alpha$  and  $\beta\text{PbO}_2$  in contrast to the coating on pure Pb that consisted mainly of tetragonal  $\text{PbO}$  as mentioned earlier.

As anodizing and cycling of the antimonial alloy continued, the capacity increased, and the coating remained firmly attached to the metal surface. After seven cycles the



(a) Outlines of the  $\text{PbSO}_4$  crystals which are retained after oxidation. The coating at this stage is still largely tetragonal  $\text{PbO}$ .

(b) Crystallites that actually make up the coating shown at higher magnifications. These are conglomerated within the original crystal volumes of the  $\text{PbSO}_4$  crystals.



(a) Outlines of  $\text{PbSO}_4$  crystals clearly shown by large features of the coating, also shown in Fig. 2. However, these crystals have been converted to  $\beta\text{PbO}_2$ .



(b) Hedgehog type of dendritic growth assumed by the  $\text{PbO}_2$  shown at higher magnification. The coating is porous and not firmly bound to the substrate.

Fig. 7 - Electron micrographs of carbon replicas of the coating on pure Pb after seven cycles

coating appeared to be a layered composite of very small crystals resembling an eutectic crystallization (Fig. 9). Trace B of the x-ray diffraction examination in Fig. 5 showed a weak pattern of  $\beta\text{PbO}_2$  with broad lines. The extra line at  $28.3^\circ$  arose from  $\alpha\text{PbO}_2$ , and some minor amount of  $\text{PbSO}_4$  was also present.

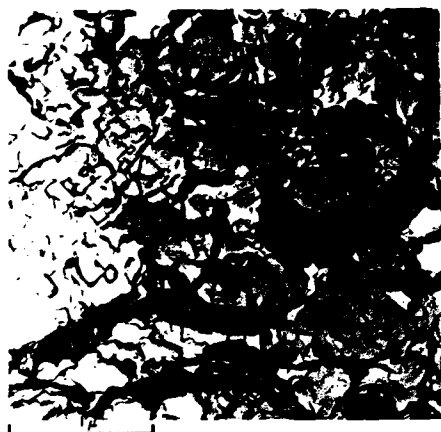


Fig. 8 - Electron micrograph of a carbon replica of the anodic coating on pure Pb after 22 cycles. The spheroidal particles, conglomerates of anhedral crystals, are not firmly attached to the electrode surface, nor do they appear to be bonded to each other.

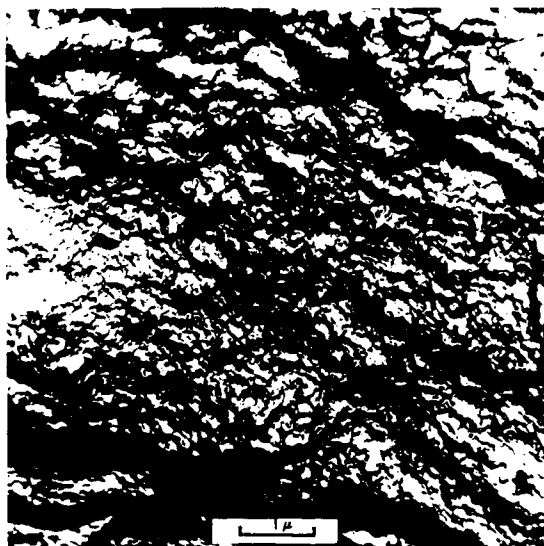


Fig. 9 - Electron micrograph of a carbon replica of the anodic coating on the Pb-Sb alloy after seven cycles. This deposit appears to be a layered composite of small crystals of  $\alpha$  and  $\beta$ - $\text{PbO}_2$ . The coating at this stage is firmly bound to the metal surface and resembles an eutectic type of crystallization of the two phases.

By comparing the electron micrographs of Figs. 2 and 7 with that of Fig. 9 and the x-ray diffraction traces shown in Fig. 5 a marked difference is seen in the morphology as well as the intensities of the diffraction patterns of the  $\text{PbO}_2$  formed on pure and antimonial Pb at this stage of cycling. The low intensity of the diffraction pattern from the antimonial coating may result from the high x-ray absorption coefficient of Pb and

the compact nature of the coating. Only crystals in the outermost layer of the tight coating can take part in the diffraction process. On the pure Pb surface, however, the coating is more porous so that many more crystals may contribute to the diffracted rays, and the diffraction pattern is thus more intense.

After 23 cycles, the anodic deposit on the antimonial electrodes consisted of larger crystals embedded in a compact primary layer of finer crystals (Fig. 3). When the coating reached this stage, it began to crack and the edges curled away from the electrode surface, although the coating remained attached to the electrode. After drying, these flakes were readily lifted from the surface with a knife edge. As described previously, the outer surface of these flakes is relatively richer in  $\beta\text{PbO}_2$  than the smoother back surface, but this back surface contains more of the beta phase than the coating that remains intact on the metal surface. As the  $\beta\text{PbO}_2$  crystals grow in size, they exert sufficient stress to break many of the mechanical bonds to the underlying eutectoidal bed of  $\alpha$  and  $\beta\text{PbO}_2$  crystals. The morphology shown in Fig. 3 further suggests that certain crystals in the initial anodic coatings fortuitously lie with preferred growth planes available to the solution interface, and during cycling of the electrodes these crystals have grown preferentially.

Starodubtsev and Timokhina (28) have shown that, in a conglomeration of NaCl crystals, bridges form only between like crystal faces and not necessarily at points of interparticle contact. The bonding between  $\text{PbO}_2$  crystals may also be between only identical crystallographic planes. In this case, the primary coatings would bond to the outer layers only through  $\beta\text{PbO}_2$  bridges, and these would form only between crystals of like orientation. On pure Pb, the primary coating on the metal is mainly  $\alpha\text{PbO}_2$  which is not isomorphous with  $\beta\text{PbO}_2$ ; hence, few such bonding points would be available. On the other hand, the eutectoidal mixture of  $\alpha$  and  $\beta\text{PbO}_2$  on the Sb alloy would present more numerous points for intercrystalline bridge formation.

**Lead Sulfate**—On the antimonial alloy, the  $\text{PbSO}_4$  coating which formed during the open circuit stand for 30 min was made up of rhomboidal crystals of  $\text{PbSO}_4$  (Fig. 10). At some intercrystalline boundaries, clusters of radiating acicular crystals appeared. The larger crystals were several microns in diameter and appeared to be implanted in a bed of smaller crystals ranging in size down to approximately  $0.1\mu$ . These coatings are very similar to those observed on pure Pb surfaces (7,9,10,12).

At 0.5- and 2-min discharge, no  $\text{PbSO}_4$  crystals or nuclei could be identified in the electron micrographs, and the coating had the same appearance as the fully charged electrode (Fig. 9). This is not unexpected because the critical nuclei of  $\text{PbSO}_4$  are very small, about 11 Å diameter (29).

Once the critical nuclei of  $\text{PbSO}_4$  are formed, however, they grow very rapidly. These initial crystals are parallel growths of the basal pinacoid, (Fig. 11). The larger crystal has a hopper type of face development, and the overlapping plates in the string are connected by bridges.

The side view in Fig. 12 shows that the  $\{210\}$  prism faces are not developed, that the platelets are usually less than  $0.5\mu$  thick, and that the interplate attachments are small bridges resulting from growth in the  $201$  and  $011$  directions. These bridges have formed between the basal planes, illustrating the principle enunciated by Starodubtsev and Timokhina (28) that bridging occurs only between like faces. Therefore, growth in the  $001$  direction is inhibited but may result from absorption of an Sb species on the  $(001)$  face. Although domes appear on some of these basal plates, the pinacoids  $(100)$  and  $(010)$  are absent, indicating that growth in these directions was most rapid. Although an effort was made to observe these crystals at an earlier stage when they could be expected to display these faces, they had grown themselves out of existence by the time the electrodes were examined, i.e. at 3.25 and 4 min.





(a) Larger prismatic crystals implanted in a layer of smaller crystals. In the center of the photograph, the bed of small crystals is seen through the "overhang" of the replicas of the larger crystals, and the line of contact between the two types of crystal is visible.



(b) Tufts of radiating acicular crystals appearing at some intercrystal boundaries

Fig. 10 - Electron micrographs of carbon replicas of  $\text{PbSO}_4$  coatings formed on Pb-Sb alloy on open circuit for 30 min in 1.2549 sp gr  $\text{H}_2\text{SO}_4$



NOT REPRODUCIBLE

(a) Hopper type of face development as illustrated by the large crystal. In the string of smaller crystals several interplate bridges are visible, and one of the basal pinacoids is modified by the {201} domes. These crystals stand out in relief from the layer of  $\text{PbO}_2$ , and only the most prominent features of this layer are replicated here.

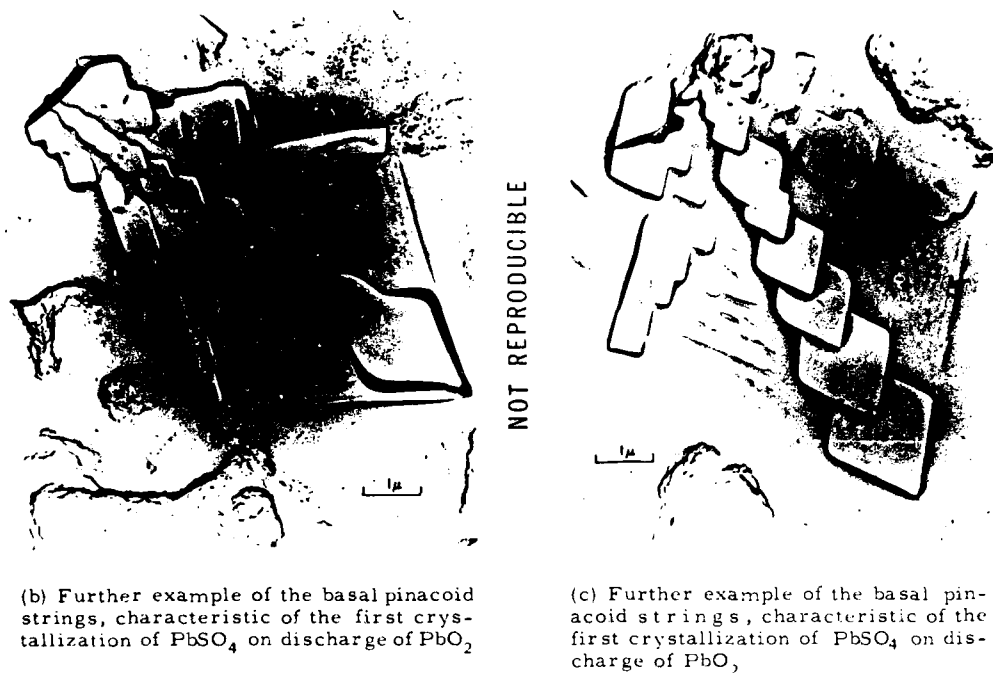


Fig. 11 - Electron micrographs of carbon replicas of  $\text{PbSO}_4$  crystals formed on the discharging antimonial electrode at 5 min, immediately following the coup de fouet

When discharged to 0.8 V vs the reference electrode, corresponding to the cutoff voltage of the positive plate of the lead-acid cell, the  $\text{PbSO}_4$  crystals exhibited a different morphology (Fig. 13). These crystals appear to be the typical prisms, parallel to the crystallographic axes, which are described for many mineral specimens. They resemble the crystals forming on self discharge of pure Pb anodes (10). These crystals lie implanted in the  $\text{PbO}_2$  layer and could not have grown from the original strings of basal plane crystals formed on the electrodes (Fig. 11). Those platelets lying in the electrode surface on their sides as shown in Fig. 12 may grow into the prisms appearing at the end of discharge (Fig. 13). On the otherhand, some residual basal pinacoids were observed (Fig. 14). The appearance of these crystals suggests that during discharge this crystal form became energetically unstable, and began to dissolve; hence, few remained at the end of discharge. Some of the anomalies associated with aging of chemically prepared  $\text{PbSO}_4$  may result from similar transformations (30-32).

The micrographs indicate that the  $\text{PbSO}_4$  crystals are several orders of magnitude larger than the  $\text{PbO}_2$  crystals and that  $\text{PbSO}_4$  does not completely cover the electrode surface at the end of discharge. The observations of this study support the conclusions of other investigators (13,14,33) that the reaction takes place by way of the solution. The end of discharge of  $\text{PbO}_2$  on pure Pb has been suggested as being the result of a covering over of the surface by  $\text{PbSO}_4$  (13). This is borne out by the electron micrographs shown in Fig. 15. In the case of  $\text{PbO}_2$  discharging on the Pb-Sb alloy, the electron micrographs, Fig. 13, suggest that nucleation and growth of the  $\text{PbSO}_4$  crystals take place at "active centers" and that the termination of discharge might be said to result from an "exhaustion or covering over of the active centers."



(a) NOT REPRODUCIBLE



(b)



(c)



(d)

Fig. 12 - Discharging electrode as in Fig. 11. Side views of the basal pinacoid plates show the interplate bridging, and the limited development of the  $\{210\}$  prism faces indicates inhibited growth in the  $c_0$  direction. Most of these platelets are less than  $0.5\mu$  thick.

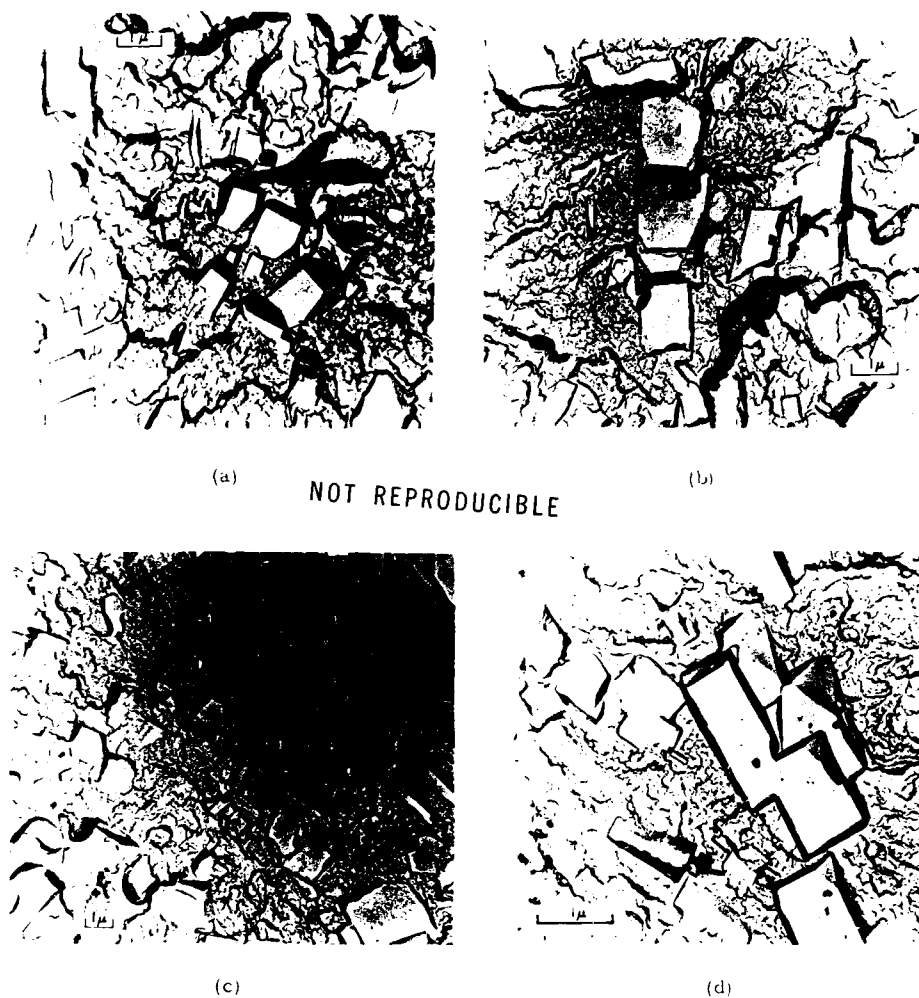


Fig. 13 - Electron micrographs of  $\text{PbSO}_4$  crystals on the surface of an antimonial electrode discharged to 0.8 V vs the  $\text{Hg}, \text{Hg}_2\text{SO}_4$  reference. At the end of discharge the  $\text{PbSO}_4$  crystals are implanted in the  $\text{PbO}_2$  coatings. Much of the  $\text{PbO}_2$  surface appears to remain available for discharge. Where the line of contact between the two phases is visible, the irregular outline indicates that the "activity" of the  $\text{PbO}_2$  varies over the surface and suggests that only certain areas take part in the discharge. A comparison with Figs. 11 and 12 suggests that these crystals may have grown from the basal pinacoids lying on their sides in the  $\text{PbO}_2$  coating as shown in Fig. 12 but not from the plates lying essentially parallel to the surface as in Fig. 11.

Another possible cause of the termination of discharge on the Sb alloy may be a limited growth rate of the  $\text{PbSO}_4$  crystals themselves. Since the slow-growing faces ultimately enclose a crystal, if the growth rate of the  $\text{PbSO}_4$  crystals is significantly retarded, accretion of additional material may not be able to keep pace with the electrochemical reaction. In this case supersaturation of Pb ions in solution would increase.

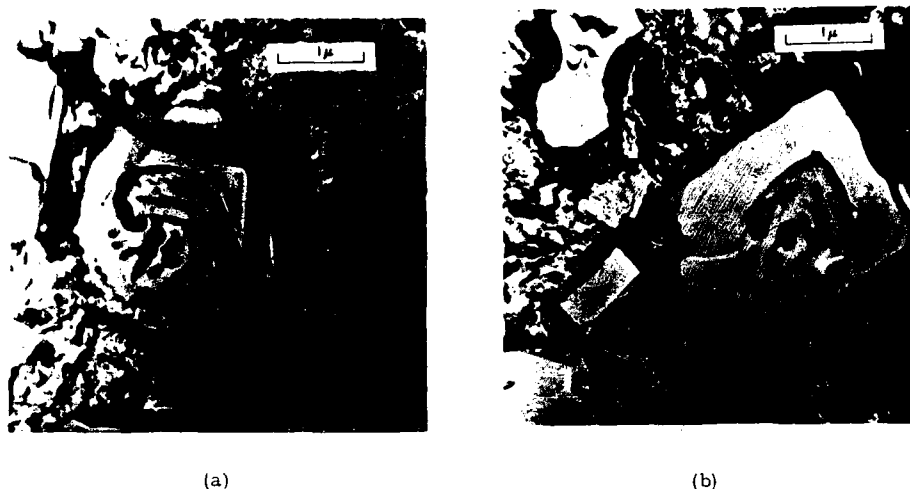


Fig. 14 - Electron micrographs of carbon replicas of vestigial basal pinacoids on the surface of an antimonial electrode at the end of discharge. The etched appearance of the edges, and labyrinthine interior suggests that these crystals have been dissolving during the discharge, rather than growing. Not many of the basal pinacoids were observed at the end of discharge, suggesting that they are a metastable form and recrystallize during the discharge period.

At this magnification, the  $\text{PbO}_2$  is seen to be heavily pitted in the immediate vicinity of these  $\text{PbSO}_4$  crystals. This would be expected if the reaction takes place by way of solution. This may have been one of the original "active" areas of  $\text{PbO}_2$  where  $\text{PbSO}_4$  was first nucleated on the electrode.

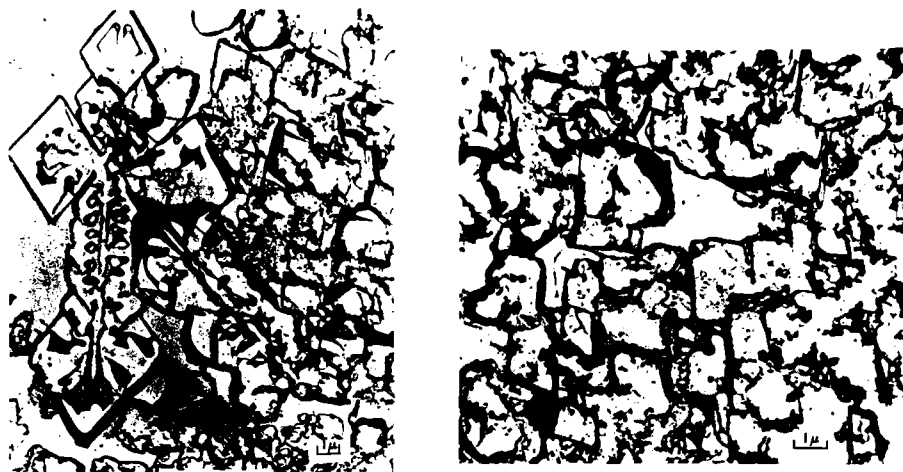
The nucleation overvoltage associated with less active centers may require excessive polarization, and the discharge would then be terminated to avoid secondary electrochemical reactions and homogeneous nucleation of  $\text{PbSO}_4$  in the solution. The possibility that the crystal growth rate may limit the discharge is further supported by the fact that additional discharge capacity is usually available from the electrode at reduced current densities. A crystal-growth control mechanism has been established for the deposition of  $\text{PbSO}_4$  on pure Pb in 2N  $\text{H}_2\text{SO}_4$  (19,34). Similar potentiostatic studies of the  $\text{PbO}_2$  electrode discharge on antimonial lead would be of interest to further clarify the mechanism.

#### A Proposed Mechanism for the Beneficial Action of Antimony on the Stabilization of Polycrystalline Lead Dioxide

To maintain structural stability in the presence of a liquid phase, a solid-solid intergranular contact must possess a lower energy than the liquid-solid contact; otherwise, the liquid will spread incidiously between grains and destroy the strength of the polycrystalline mass (35,36). It has been shown that, relatively,

$$\sigma_{s s} = 2\sigma_{l s} \cos \theta/2,$$

where  $\sigma_{s s}$  is the free energy of contact between two contiguous grains of the same material and  $\sigma_{l s}$  is the interfacial energy associated with the phase boundary between



(a) General outline of the basal pin-acoid as visible in the radiating dendritic cluster; however, the faces are severely distorted. The radiating spikes are implanted in a passivating coating of intergrown rhomboidal crystals.

(b) Passivating coating of intergrown crystals of  $\text{PbSO}_4$  which essentially covers the surface. The differences between the  $\text{PbSO}_4$  crystals at the end of discharge on the Sb-Pb alloy may be seen by comparing this photograph with those shown in Fig. 13.

Fig. 15 - Electron micrographs of carbon replicas of  $\text{PbSO}_4$  crystals remaining on the surface of a pure Pb electrode after discharge of an anodic  $\text{PbO}_2$  coating

the liquid and solid. The angle  $\theta$  is the dihedral angle of penetration which the liquid makes between two contiguous grains.

Considerable solid-solid contact may be maintained in the presence of relatively large volumes of liquid if  $\sigma_{ss} < 2\sigma_{sl}$ . Furthermore, growing crystals will not weld to each other unless the energy of intergranular contact is less than twice the solid-liquid interphase energy. If  $\theta$  is  $120^\circ$  or more, the intercrystalline boundary may be adjudged thermodynamically stable. But as  $\theta$  approaches  $0^\circ$ , the liquid will inexorably replace the solid-solid contact. If a sufficient number of such high-energy boundaries are present in a polycrystalline aggregate permeated by a liquid, the mass will disintegrate. These relations are indicated schematically in Fig. 16.

The morphology of  $\text{PbO}_2$  particles may vary from spheroidal to prismatic, and the relative stability of the mass is related to these structures (37). Although the magnitude of the relative interface energy of  $\text{H}_2\text{SO}_4$  on  $\text{PbO}_2$  is not known, at an air interface, the surface tension of  $\text{H}_2\text{SO}_4$  solutions has been shown to vary with the concentration, as indicated in Fig. 17 (38). The interfacial energy of  $\text{H}_2\text{SO}_4$  on  $\text{PbO}_2$  is probably a similar function of concentration, and the disintegration of the active mass may be expected to take place more readily in more dilute and very concentrated solutions. The positive-plate active material is not rigidly confined and is free to adjust to such structural changes. As interparticle boundaries become replaced with a liquid phase, the overall volume of the solid would appear to increase and thus account in part for the loss of apparent density of the active mass during cell operation, Fig. 18 (3).

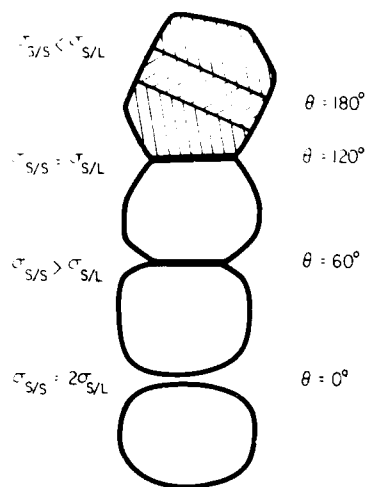
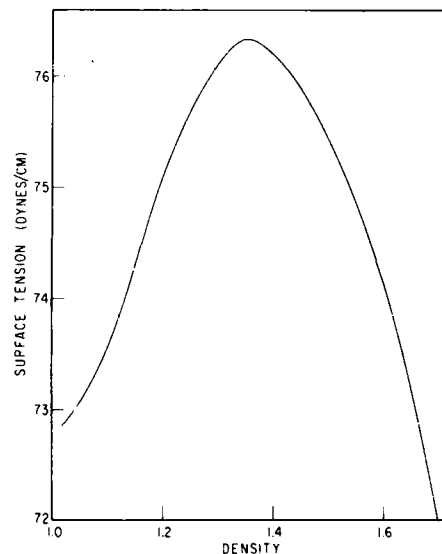


Fig. 16 - Schematic diagram of the interphase boundaries in polycrystalline materials in contact with a liquid phase. The dihedral angle of penetration of the liquid at the grain boundaries is a function of the relative surface layer free energies associated with contiguous grains. Twin boundaries and boundaries with crystallographic near-match of atomic reticulate structure characteristically possess relatively low energy; hence, they are stable and not subject to intergranular attack. This is indicated at the top of the diagram. As the relative interparticle free energies increase, the penetration of the liquid between grains becomes greater, and the particles may become completely separated, indicated at the bottom of the drawing.

Fig. 17 - The relation of surface tension and concentration of aqueous  $H_2SO_4$  solutions at 20°C (38)



In a polycrystalline mass, interparticle contacts of varying energy will be present because of variation of contiguous grain misorientations (39), which leads to differences in the rate and extent of attack at the grain boundaries. During operation of the lead-acid cell, pockets of active material may become electrically isolated from each other as the more "reactive" boundaries are replaced with electrolyte. This mode of plate failure has been observed by Bode and Euler using radioactive tracers (40).

During positive-plate operation the concentration of the  $H_2SO_4$  changes, and the lower surface tension of more dilute solutions (Fig. 17) suggests that in the pores of the plates, where the most dilute solution forms, it may attack intercrystalline boundaries that might

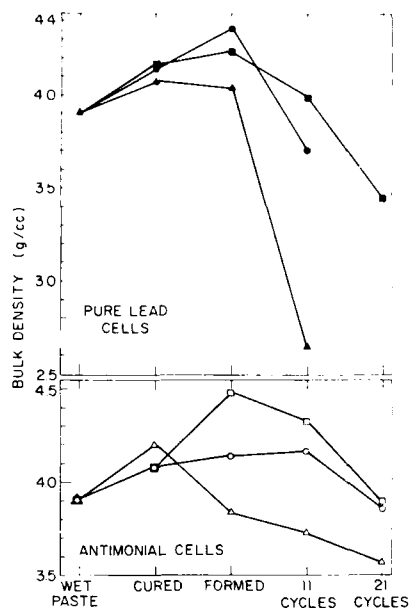


Fig. 18 - Bulk density changes with cycling of the positive active material in pure Pb and Pb-Sb cells. The rate of density loss is markedly greater for the pure Pb cells (3).

be stable in more concentrated solutions. This may account, in part at least, for the relatively more destructive influence of deep cycling on positive plates (41).

The stabilization of the positive active material in nonantimonial cells by prolonged shallow discharge, known as "trickle discharge," has been attributed to the formation of interlocking splines of  $\text{PbSO}_4$  (42). Introduction of the second solid phase,  $\text{PbSO}_4$ , necessitates consideration of the interphase energies of  $\text{PbO}_2/\text{PbSO}_4$ ,  $\text{PbSO}_4/\text{PbSO}_4$ , and  $\text{H}_2\text{SO}_4$ . The solid phase  $\text{PbSO}_4$  may act as a grain boundary cement, giving rise to sutured grain boundaries, or it may form bridging crystals from grain to grain of  $\text{PbO}_2$ , similar to muscovite mica in flexible sandstone (43) or hercynite ( $\text{FeAl}_2\text{O}_4$ ) in magnesio-wüstite ceramics (36), depending on the relative interphase energies.

The electrode surface is the preferred site for crystallization only under the conditions where the relative interphase energies have the necessary relationships (44). The conclusion can be drawn from the experimental evidence of this and previous studies that Sb lowers the relative intergranular contact energy between particles of  $\text{PbO}_2$  grown in  $\text{H}_2\text{SO}_4$  so that a compact welded mass of crystals is produced. These relative energies are indicated schematically in Fig. 19. It is suggested that Sb acts in this manner by substitutional solid solution in the  $\text{PbO}_2$  lattices. The Sb ions may enter only the surface layers of the  $\text{PbO}_2$  crystals, and markedly lower the surface-layer free energy. The superior strength of the polycrystalline mass of  $\text{PbO}_2$ , the coherent nature of the corrosion product on Pb-Sb alloys, and the bonding between the grid and the active material pellets characteristic of antimonial cells are attributed to this mechanism. In addition the eutectoidal mass of  $\alpha$  and  $\beta\text{PbO}_2$  formed on the antimonial alloys indicates that Sb also promotes bonding between the two polymorphs. Elementary crystal chemical considerations indicate that this is a feasible mechanism.



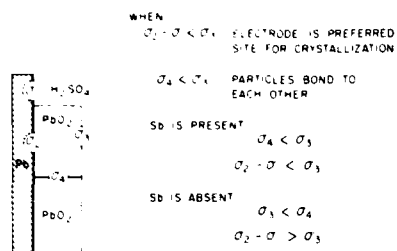


Fig. 19 - Schematic representation of the relative interphase free energies at the Pb anode, where  $\sigma_1$  = Pb/electrolyte interface,  $\sigma_2$  = Pb/PbO<sub>2</sub> interface,  $\sigma_3$  = PbO<sub>2</sub>/electrolyte interface, and  $\sigma_4$  = PbO<sub>2</sub>/PbO<sub>2</sub> interface. As indicated to the right of the diagram, the adhesion and cohesion of the anodic coating depends on these relative interphase energies.

### Some Crystal Chemistry Considerations

Lead and antimony form oxides that crystallize in oxygen octahedra with a metal ion coordination number of six (45). The crystal structures of these materials are largely determined by the packing of the octahedra which are usually joined by sharing edges and corners. In tetragonal  $\beta$ -PbO<sub>2</sub>, strings of PbO<sub>6</sub> octahedra lie parallel to the  $c_0$  axis as in the rutile structure. In orthorhombic  $\alpha$ -PbO<sub>2</sub> (46,47) the linkages between octahedra are also through sharing edges and corners in chains parallel to the  $a_0$  axis in the pattern of columbite (48). The generic or type names for these structures are rutile (or cassiterite), tri-rutile (or tapiolite), and columbite. In addition to Pb and Sb several other metals form oxides that crystallize in this manner. Some compounds having these structures are listed in Table 2 (45,49). Among these oxides are many of mixed valence required to maintain statistical electrical neutrality in structures that have twice as many oxygen atoms as metal atoms. Hund (50) has discussed this stoichiometric requirement in some detail, and researchers have shown that the rutile structure may accommodate simultaneously more than one kind of guest ion to maintain the metal/oxygen ratio (49-52). The relative mole ratios are listed in Table 3 for such mixed oxides. In some instances a continuous series of solid solutions of the mixed oxides may be formed.

Table 4 gives the ground state electron structures and ionic radii (53,54) of the metals of interest. Tetravalent Pb has a radius of 0.83 Å; therefore, potentially, many mixed oxides of PbO<sub>2</sub> and these other metals may be synthesized. The action of Sb in the positive active material of the lead-acid cell has been proposed to be a result of substitutional solid solution in the PbO<sub>2</sub>. Because both tri- and pentavalent Sb are smaller in size than the Pb ion, the oxygen octahedra enclosing the Sb ions are more compact, the lattice energy would be increased, and the surface energy decreased, resulting in a more stable, harder crystal. A similar incorporation of Sb and Ni oxides in TiO<sub>2</sub> (rutile) has been reported (51,52), and other inorganic pigments have been developed by dissolving stoichiometric ratios of other oxides in the rutile-type oxides, TiO<sub>2</sub> and SnO<sub>2</sub> (50).

More interest has probably not been shown in PbO<sub>2</sub>-related oxides because synthesizing by the usual ceramic techniques of compacting and sintering mixed powders may not be used since PbO<sub>2</sub> has a relatively low thermal decomposition temperature of approximately 300°C in air (55). However, many of the possible oxides may be synthesized by aqueous electrochemical oxidation.

The conductivity of PbO<sub>2</sub> is that characteristic of metals (56-58) and is attributed to an anionic deficiency, the free electrons apparently existing under normal conditions, in a conduction band. In introducing transition metals into such a structure, the effect on the conductivity of the oxide is difficult to predict. On the other hand many of the transition metal oxides are metallic in character. This is attributed to their unfilled d bands and hybridized overlapping atomic orbitals. The metallic state in these oxides is currently being actively investigated (59-61).

Table 2  
Oxide Lattice Types

Rutile			Tri-rutile	Columbite
$\beta\text{PbO}_2$	$\text{GeO}_2$	$\text{FeSbO}_4$	$\text{CuSb}_2\text{O}_6$	$\alpha\text{PbO}$
$\text{OsO}_2$	$\beta\text{MnO}_2$	$\text{FeTaO}_4$	$\text{MgTa}_2\text{O}_6$	$\text{ReO}_2$
$\text{RuO}_2$	$\text{CrO}_2$	$\text{GaSbO}_4$	$\text{NiTa}_2\text{O}_6$	$(\text{Fe}, \text{Mn})\text{Nb}_2\text{O}_6$
$\text{SnO}_2$	$\text{CrO}_{2.14}$	$\text{MnSbO}_4$	$\text{CoTa}_2\text{O}_6$	$(\text{Fe}, \text{Mn})\text{Ta}_2\text{O}_6$
$\text{TaO}_2$	$\text{Cr}_{0.19}\text{Mo}_{0.81}\text{O}_2$	$\text{TiVO}_4$	$\text{FeTa}_2\text{O}_6$	$\text{Mn}, \text{Nb}_2\text{O}_6$
$\text{TeO}_2$	$\text{Cr}_{0.33}\text{Mo}_{0.67}\text{O}_2$	$\text{SbVO}_4$	$\text{MgSb}_2\text{O}_6$	$\text{MgNb}_2\text{O}_6$
$\text{TiO}_2$	$\text{AlSbO}_4$	$\text{VSbO}_4$	$\text{NiSb}_2\text{O}_6$	$\text{NiNb}_2\text{O}_6$
$\text{WO}_2$	$\text{CrNbO}_4$	$\text{RhNbO}_4$	$\text{CoSb}_2\text{O}_6$	$\text{CoNb}_2\text{O}_6$
$\text{NbO}_2$	$\text{CrSbO}_4$	$\text{RhTaO}_4$	$\text{FeSb}_2\text{O}_6$	$\text{FeNb}_2\text{O}_6$
$\text{MoO}_2$	$\text{CrTaO}_4$	$\text{RhVO}_4$	$\text{ZnSb}_2\text{O}_6$	$\text{ZnNb}_2\text{O}_6$
$\text{IrO}_2$	$\text{FeNbO}_4$	$(\text{Fe}, \text{Ta}, \text{Nb})\text{O}_2$	$(\text{Fe}, \text{Mn})(\text{Ta}, \text{Nb})_2\text{O}_6$	$\text{ZnTa}_2\text{O}_6$
				$\text{MnTa}_2\text{O}_6$
				$\text{MnSb}_2\text{O}_6$

Table 3  
Stoichiometric Ratio of Oxides  
( $A + B = \text{MeO}_2$ )\*

A	B	
$\text{Me}_2\text{O}$	$3\text{Me}_2\text{O}_5$	$3\text{MeO}_3$
$\text{MeO}$	$\text{Me}_2\text{O}_5$	$\text{MeO}_3$
$\text{Me}_2\text{O}_3$	$\text{Me}_2\text{O}_5$	$\text{MeO}_3$

\*Me = metal.

The geometrical considerations in selecting possible guest ions for the  $\text{PbO}_2$  lattices indicate that the cation/anion radius ratio should be between 0.4 and 0.7. These ratios are given for the metals listed in Table 4. The ratio having the greatest stability is the lower limit (54), and for this reason ions smaller than  $\text{Pb}^{4+}$  should be most effective in imparting beneficial structural properties to the polycrystalline mass of  $\text{PbO}_2$ . There are other oxide structures that are of interest because of their possible electrochemical magnetic and semiconducting properties. These include the perovskite (62,63) and tungsten bronze (64-66) type structures. The bronzes of lead with tungsten and vanadium have been prepared (67,68), but they have not been studied from an electrochemical viewpoint. It is only recently that any of these bronzes has been the subject of electrochemical investigation (69-71).

From a thermodynamic view, some of the lower-valence metal ions may be unstable at positive plate potentials in the lead-acid cell. However, when incorporated in the  $\text{PbO}_2$  lattice, the crystal chemical considerations probably would prevent further oxidation.

Table 4  
Ionic Radii and Electron Structure of Metals Potentially  
Compatible With Lead Dioxide Lattices

Ion	Valence	Atomic Electron Structure	$r_c$ (Å)	$r_c/r_{ox}$
Al	3	(Ne)3s <sup>2</sup> 3p <sup>1</sup>	0.57	0.43
As	5	(Ar)3d <sup>10</sup> 4s <sup>2</sup> 4p <sup>3</sup>	0.47	0.33
Bi	3	(Xe)4f <sup>14</sup> 5d <sup>10</sup> 6s <sup>2</sup> 6p <sup>3</sup>	1.20	0.91
	5		0.74	0.56
Co	2	(Ar)3d <sup>7</sup> 4s <sup>2</sup>	0.71	0.54
	3		0.63	0.48
Cr	3	(Ar)3d <sup>5</sup> 4s <sup>1</sup>	0.64	0.48
	6		0.52	0.39
Cu	2	(Ar)3d <sup>10</sup> 4s <sup>1</sup>	0.70	0.53
Fe	2	(Ar)3d <sup>6</sup> 4s <sup>2</sup>	0.76	0.58
	3		0.67	0.51
Ga	3	(Ar)3d <sup>10</sup> 4s <sup>2</sup> 4p <sup>1</sup>	0.64	0.48
Ge	4	(Ar)3d <sup>10</sup> 4s <sup>2</sup> 4p <sup>2</sup>	0.56	0.42
Hf	4	(Xe)4f <sup>14</sup> 5d <sup>2</sup> 6s <sup>2</sup>	0.81	0.61
In	3	(Kr)4d <sup>10</sup> 5s <sup>2</sup> 5p <sup>1</sup>	0.81	0.61
Ir	4	(Xe)4f <sup>14</sup> 5d <sup>7</sup> 6s <sup>2</sup>	0.65	0.49
Li	1	He 2s <sup>1</sup>	0.60	0.45
Mg	2	(Ne)3s <sup>2</sup>	0.70	0.53
Mn	2	(Ar)3d <sup>5</sup> 4s <sup>2</sup>	0.80	0.61
	3		0.72	0.55
	4		0.56	0.42
Mo	4	(Kr)4d <sup>5</sup> 5s <sup>1</sup>	0.67	0.51
Nb	4	(Kr)4d <sup>4</sup> 5s <sup>1</sup>	0.70	0.53
	5		0.68	0.52
Ni	2	(Ar)3d <sup>8</sup> 4s <sup>2</sup>	0.68	0.52
	3		0.62	0.47

Table 4 continues

Table 4 (continued)  
Ionic Radii and Electron Structure of Metals Potentially  
Compatible With Lead Dioxide Lattices

Ion	Valence	Atomic Electron Structure	$r_i$ (Å)	$r_i / r_{\text{ox}}$
Os	4	(Xe)4f <sup>14</sup> 5d <sup>6</sup> 6s <sup>2</sup>	0.67	0.51
Pb	2	(Xe)4f <sup>14</sup> 5d <sup>10</sup> 6s <sup>2</sup> 6p <sup>2</sup>	1.18	0.89
	4		0.83	0.63
Re	4	(Xe)4f <sup>14</sup> 5d <sup>5</sup> 6s <sup>2</sup>	0.66	0.50
Rh	3	(Kr)4d <sup>8</sup> 5s <sup>1</sup>	0.68	0.52
Ru	4	(Kr)4d <sup>7</sup> 5s <sup>1</sup>	0.65	0.49
Sb	3	(Kr)4d <sup>10</sup> 5s <sup>2</sup> 5p <sup>3</sup>	0.71	0.54
	5		0.66	0.50
Sc	3	(Ar)3d <sup>1</sup> 4s <sup>2</sup>	0.81	0.61
Sn	4	(Kr)4d <sup>10</sup> 5s <sup>2</sup> 5p <sup>2</sup>	0.73	0.55
Ta	4	(Xe)4f <sup>14</sup> 5d <sup>3</sup> 6s <sup>2</sup>	0.70	0.53
Te	4	(Kr)4d <sup>10</sup> 5s <sup>2</sup> 5p <sup>4</sup>	0.87	0.66
	6		0.56	0.42
Ti	3	(Ar)3d <sup>2</sup> 4s <sup>2</sup>	0.67	0.51
	4		0.64	0.48
V	3	(Ar)3d <sup>3</sup> 4s <sup>2</sup>	0.64	0.48
	4		0.60	0.45
	5		0.59	0.45
W	4	(Xe)4f <sup>14</sup> 5d <sup>4</sup> 6s <sup>2</sup>	0.68	0.52
	6		0.68	0.52
Zn	2	(Ar)3d <sup>10</sup> 4s <sup>2</sup>	0.72	0.55
Zr	4	(Kr)4d <sup>2</sup> 5s <sup>2</sup>	0.80	0.61
O	-2	He 2s <sup>2</sup> 2p <sup>4</sup>	1.32	—

The Atlas of Electrochemical Equilibria (72) and Latimer's book (73) are handy reference guides for assessing the thermodynamic stability of proposed dopant oxides. For application in the lead-acid cell, toxicity is an important consideration, particularly for service in confined spaces. Elements likely to give volatile toxic compounds under operating cell conditions would not be of interest; for example, Os forms volatile, toxic  $\text{OsO}_4$  that could occur at the positive plate of the cell. Arsenic forms the poisonous gas arsine at negative plate potentials and thus is not suitable for such applications.

#### An Outline for Future Investigations

The complex nature of the electrochemical operation of the  $\text{PbO}_2$ ,  $\text{PbSO}_4$  electrode has been indicated by the large number of areas touched on in this report. The suggested mechanism of the action of Sb in the electrode indicates the most profitable direction for future investigation.

Present theory is inadequate to predict with certainty what elements will substitute for Sb and the experimental approach must thus be somewhat empirical. The large number of elements that should form solid solutions in the  $\text{PbO}_2$  lattices are listed in Table 4. In selecting those that appear most likely to act in the same manner as Sb, metals with the smallest ionic radii should receive first attention. In addition, combinations of elements should be considered. These should be in ratios that can give the stoichiometry of  $\text{PbO}_2$  as indicated in Table 3.

Although it is not possible to prepare these materials by the customary fusion methods, they may be incorporated in PbO by fusion, and this in turn may be used to fabricate pasted electrodes in the usual fashion. The dopant oxide may also simply be mixed in a paste with PbO and enter the  $\text{PbO}_2$  lattice during anodic oxidation, as Sb does.

Quite aside from the immediate practical goal of finding a substitute for Sb in the lead-acid cell, a survey of these oxides may offer new electrochemical systems or new oxides of magnetic or semiconductor interest. For example, the tungsten bronzes have remarkable chemical and electrical characteristics, and they might serve as electrodes in many kinds of cell, including those with aqueous and molten salt electrolytes. A broad program of investigation of the physical and electrochemical properties of these oxides would be of great scientific interest and holds promise of uncovering new electrode materials.

#### ACKNOWLEDGMENT

The spectrographic analyses given in Table 1 were kindly supplied by Mr. S. H. Cress of the Analytical Chemistry Branch, Central Materials Research Facility of the Naval Research Laboratory, Washington, D.C.

## REFERENCES

1. D. Kordes, *Chemie-Ing.-Tech.* 38, 638 (1966)
2. J. Burbank, *J. Electrochem. Soc.* 111, 1112 (1964)
3. E.J. Ritchie and J. Burbank, *J. Electrochem. Soc.* 117, 299 (1970)
4. J. Burbank, "Cycling Anodic Coatings on Pure and Antimonial Lead in  $H_2SO_4$ ," paper presented at 7th International Power Sources Symposium, Sept. 15-17, 1970, Brighton, Eng.
5. J. Burbank, *J. Electrochem. Soc.* 118, 525 (1971)
6. L.M. Levinzon, I.A. Aguf, and M.A. Dasoyan, *J. Appl. Chem. USSR* 39, 525 (1966). Note: In this English translation of Zhur. Prikl. Khim 39, 556 (1966) parts (a) and (b) of Fig. 5 are reversed
7. D. Pavlov, *Ber. Bunsengesht. physik. Chem.* 71, 398 (1967)
8. D. Pavlov, C.N. Poulieff, E. Klaja, and N. Iordanov, *J. Electrochem. Soc.* 116, 316 (1969)
9. W. Feitknecht and A. Gaumann, *J. Chim. Phys.* 49, C135 (1952)
10. W. Feitknecht, *Z. Elektrochem.* 62, 795 (1958)
11. I.I. Astakhov, E.S. Vaisberg, and B.N. Kabanov, *Bull. Acad. Sci. USSR* 154, 194 (1954)
12. D. Pavlov, *Electrochim. Acta* 13, 2051 (1968)
13. B.N. Kabanov, D.I. Leikis, and E.I. Krepakova, *Doklady Akad. Nauk S.S.S.R.* 98, 989 (1954)
14. S. Hisano, *Kogyo Kagaku Zasshi* 62, 376 (1959)
15. H.B. Mark, Jr., *J. Electrochem. Soc.* 109, 634 (1962)
16. A.C. Simon, *Electrochem. Technol.* 1, 82 (1963)
17. D. Berndt and E. Voss, *Batteries 2* (D.H. Collins, editor), Pergamon, New York, 1965, p.17
18. M. Fleischmann and H.R. Thirsk, Chapter 3 in *Advances in Electrochemistry and Electrochemical Engineering* (P. Delahay, editor), Vol. 3, Interscience, New York, 1963, p. 123
19. D.A. Vermilyea, Chapter 4 in *Advances in Electrochemistry and Electrochemical Engineering* (P. Delahay, editor), Vol. 3, Interscience, New York, 1963, p.211
20. W.F. Hillebrand, G.E.F. Lundell, H.A. Bright, and J.I. Hoffman, Chapter 14 in *Applied Inorganic Analysis*, 2nd ed., Wiley, New York, 1953
21. J.L. Dawson, J. Wilkinson, and M.I. Gillibrand, *J. Inorg. Nucl. Chem.* 32, 501 (1970)

22. H.P. Klug, and L.E. Alexander, X-Ray Diffraction Procedures for Polycrystalline and Amorphous Materials, Wiley, New York, 1954
23. D.E. Bradley, J. Appl. Phys. 27, 1399 (1956)
24. E.F. Fullam, Symposium on Techniques for Electron Metallography, Special Technical Publication 155, Am. Soc. Testing Mater. Philadelphia, 1954, p. 101
25. J. Burbank, Trans. A.I.M.E. 197, 55 (1953)
26. J. Burbank, in Power Sources 1966 (D.H. Collins, editor), Pergamon, New York, 1967, p. 147
27. J. Burbank, "The Plate Materials of the Lead-Acid Cell, Part 3—Anodic Oxidation of Tetragonal PbO," NRL Report 6613, Dec. 29, 1967
28. S.V. Starodubtsev and N.I. Timokhina, Doklady Akad. Nauk SSSR 62, 619 (1948)
29. A.G. Walton, Mikrochim. Acta 1963, 422 (1963)
30. L.B. Nelson, "Crystal Growth and Isotopic Exchange of Lead Sulfate in Aqueous Media," Dissertation Abstr. 16, 36 (1956); New York University, 1955
31. I.M. Kolthoff and B. van't Riet, J. Phys. Chem. 63, 817 (1959)
32. I.M. Kolthoff and C. Rosenblum, J. Am. Chem. Soc. 57, 597, 607 (1935)
33. A.C. Simon, C.P. Wales, and S.M. Caulder, J. Electrochem. Soc. 117, 987 (1970)
34. M. Fleischmann and H.R. Thirsk, Trans. Faraday Soc. 51, 71 (1955)
35. C.S. Smith, Trans. A.I.M.E. 175, 15 (1948)
36. L.H. Van Vlack and O.K. Riegger, Trans. A.I.M.E. 224, 957 (1962)
37. J. Burbank, in Batteries (D.H. Collins, editor), Pergamon, New York, 1963, p.43
38. W. Hoffmann and F.W. Seemann, Z. Phys. Chemie N.F. 24, 300 (1960)
39. L.H. Van Vlack, "Geometry of Microstructures" in Microstructure of Ceramic Materials, National Bureau of Standards Misc. Pub. 257, Apr. 6, 1964, p. 1
40. H. Bode and J. Euler, Electrochim. Acta 11, 1211 (1966)
41. E. Voss and G. Huster, "The Effect of Depth of Discharge on the Cycle Life of Positive Lead-Acid Plates" in Performance Forecast of Selected Static Energy Conversion Devices (G.W. Sherman and L. Devol, editors), 29th Meeting of AGARD Propulsion and Energetics Panel, Liege, Belgium, June 12-16, 1967
42. J. Burbank and C.P. Wales, "The Lead Calcium Battery. Part 3—Submarine Cells," NRL Report 5773, May 29, 1962
43. R.C. DeVries and D.B. Jogle, J. Am. Ceram. Soc. 51, 387 (1968)
44. D.A. Vermilyea, "Anodic Films" in Advances in Electrochemistry and Electrochemical Engineering (P. Delahay, editor), Vol. 3, Interscience, New York, 1963, p. 211

45. R.W.G. Wyckoff, Chapters IV and IX in Crystal Structures, Interscience, New York, 1960
46. A.I. Zaslavskii, Yu. D. Kondrashov, and S. S. Tolkachev, Doklady Akad. Nauk S.S.S.R. 75, 559 (1950)
47. A.I. Zaslavskii and S.S. Tolkachev, Russ. J. Phys. Chem. 26, 743 (1952)
48. J.H. Sturdivant, Z. Krist. 75, 88 (1930)
49. K. Sasvári, Acta Phys. Acad. Sci. Hung. 11, 345 (1960)
50. F. Hund, Angew. Chem. Inter Ed. 1, 41 (1962)
51. H.B. Krause, H.W. Reamer, and J.L. Martin, Mat. Res. Bull. 3, 233 (1968)
52. H.B. Krause, Mat. Res. Bull. 3, 241 (1968)
53. K. Sasvári, Acta Phys. Acad. Sci. Hung. 11, 333 (1960)
54. R.C. Evans, An Introduction to Crystal Chemistry, 2nd ed., University Press, Cambridge, 1964
55. W.B. White, F. Dacheille, and R. Roy, J. Am. Ceram. Soc. 44, 170 (1961)
56. U.B. Thomas, Trans. Electrochem. Soc. 94, 42 (1948)
57. D.A. Frey, and H.E. Weaver, J. Electrochem. Soc. 107, 930 (1960)
58. A. Aguf, A.I. Rusin, and M.A. Dasoyan, Zashchitn. Metal. i. Oksidnye Pokrytiya, Korroziya Metal. i. Issled. v Obl. Elektrokhim., Akad. Nauk S.S.S.R., Otd. Obshch. i. Tekhn. Khim., Sb. Statei 1965, 328 (1965)
59. I.G. Austin and N.F. Mott, Science 168, 71 (1970)
60. J.A. Roberson and R.A. Rapp, J. Phys. Chem. Solids 30, 1119 (1969)
61. I.G. Austin and C.E. Turner, Phil. Mag. 19, 939 (1969)
62. A.S. Viskov, Yu. N. Venetsev, G.S. Zhdanov, and L.D. Onikienko, Soviet Phys.-Cryst. 10, 720 (1966)
63. Yu. N. Venetsev, et al., Soviet Phys. "Doklady" 9, 751 (1965)
64. M.J. Sienko, Nonstoichiometric Compounds, Advances in Chemistry Series 39, American Chemical Society, Washington, D.C., 1963, p. 224
65. H.R. Shanks, P.H. Sidles, and G.C. Danielson, Nonstoichiometric Compounds, Advances in Chemistry Series 39, American Chemical Society, Washington, D.C., 1963, p. 237
66. A.S. Ribnick, B. Post, and E. Banks, Nonstoichiometric Compounds, Advances in Chemistry Series 39, American Chemical Society, Washington, D.C., 1963, p. 246
67. R.A. Bernoff and L.E. Conroy, J. Am. Chem. Soc. 82, 6261 (1960)
68. J. Darriet, R. von der Muehl, and J. Galy, Bull. Soc. fr. Minéral. Cristallogr. 92, 17 (1969)



69. J. O'M. Bockris, A. Damjanovic, and R.J. Manning, *J. Electroanal. Chem.* 18, 349 (1968)
70. D.B. Šepa, A. Damjanovic, and J. O'M. Bockris, *Electrochim. Acta* 12, 746 (1967)
71. R.S. Alwitt and A.K. Vijh, *J. Electrochem. Soc.* 117, 413 (1970)
72. M. Pourbaix, Atlas of Electrochemical Equilibria in Aqueous Solutions, Pergamon, New York, 1966
73. W. M. Latimer, The Oxidation States of the Elements and Their Potentials in Aqueous Solutions, 2nd ed., Prentice-Hall, New York, 1952